Experimental investigation of nanoparticles concentration, boiler temperature and flow rate on flow boiling of zinc bromide and acetone solution in a rectangular duct

Hayder I. Mohammed[1,2,*], Donald Giddings[2], Gavin S. Walker[3]

(1) Department of Physics, Collage of Education, University of Garmian, Kalar, Iraq

(2) Faculty of Engineering, the University of Nottingham, University Park, Nottingham NG7 2RD, UK.

(3) Faculty of Engineering, the University of Nottingham, Innovation Park, Nottingham NG7 2TU, UK.

∗ Corresponding author (Hayder I. Mohammed).

E-mail addresses: hayder.i.mohammad@garmian.edu.krd, haidarnuceng@gmail.com.

Mobile: +447459811483

Abstract

Despite the increase in heat transfer properties of nano-fluids, they are not currently used in vapour absorption refrigeration systems (VARS), and there is little literature on the flow boiling behaviour of concentrated salt solutions with nano-particle suspension. A potential novel working fluid solution for a vapour absorption refrigeration unit capable of utilising very low grade waste heat is acetone and zinc bromide, and this fluid is investigated here as the salt solution with graphene nanoparticles in suspension in flow boiling similar to that found in VARS. Nanoparticle concentration, boiler temperature, and flow rate are investigated. The Rohsenow constant in the flow boiling correlation for the nanofluid acetone / $ZnBr_2$ with graphene on a stainless steel surface is found to be 0.217. By increasing the particle concentration from 0 to 05 vol.%, heat flux and heat transfer coefficient on the heated surface increase from 8638 W/m^2 and 106 W/m^2.K to 13164 W/m^2 and 167 W/m^2.K, respectively. The steady pressure of the system increases with increasing loading of the nanoparticles and consequently the saturation temperature increases. This is because of the increased vapour generation as a consequence of improved heat transfer properties. Heat transfer coefficient is linearly proportional to temperature difference between the fluid and wall (e.g increases from 78 W/m^2.K to 145 W/m^2.K when the temperature difference increase from 102 K to 135 K) in the range tested and the heat flux correspondingly reflects a quadratic relationship with temperature difference. Increasing nanofluid flow rate reduces both the production of acetone in the condenser and the salt concentration in the strong solution reservoir. Regarding properties of the fluid, the density and the specific heat follow the simple mixture combination rule; the thermal conductivity of the nanofluid increases by 4.5 % with increasing the loading the particles to 0.5 vol. %, following reasonably well the correlation of Suganthi [1]; the viscosity increases linearly with concentration of nanoparticles (e.g increases from 3.22 m Pa.s to 4.5 m Pa.s by increasing the concentration from 0 to 0.5 vol. %) ; the stability of the nano-salt-fluid is affected by the density of the basefluid. The nanofluid showing good stability for 4 hours and during the circulation of the fluid in the rig. Over the range of temperatures tested, the salt solution demonstrates characteristics of nucleate boiling behaviour and offers significant improvement over the properties of the base fluid in terms of boiling effectiveness, indicating that it will provide improved operation in a VARS situation.

Key words

Flow boiling, heat transfer, refrigeration system, acetone / $ZnBr_2$, Graphene, nano-salt-fluid, rectangular duct, experiment.

Introduction

Flow boiling heat transfer occurs in vapour absorption refrigeration systems (VARS) as well as in various industrial areas, such as refrigeration systems in many applications, power generation, chemical engineering, high-power electronics, and nuclear reactor cooling [2]. Improvements in flow boiling heat transfer systems can improve energy efficiency and offer a route to reduce global energy consumption, e.g. in the United States, air conditioners consume 6% of electricity produced, costing annually $29 billion and 117 million metric tons of CO_2 released into the environment [3]. To improve the heat transfer of the fluid, the behaviour and the properties of the fluid itself can be enhanced. Nanofluids are an alternative to existing heat transfer fluids for thermal and industrial applications, due to their modified thermo-physical properties which can enhance the efficiency of processes such as boiling [4].

The early stages of boiling start with single phase natural convection, with heat transferred from the hot surface to the fluid; after this, nucleate boiling begins, which is a two phase natural convection process. In nucleate boiling, bubbles are created and grow from the hot surface. If the heat flux through the surface is further increased, then a layer of vapour forms between the hot surface and the liquid which is film boiling. The process between nucleate and the film boiling is transition boiling [5].

The number of studies of nanofluid boiling has increased significantly over the last decade with emphasis mainly on pool boiling [6-18] rather than flow boiling [19-26], even though flow boiling has more applications (such as boiling in microchannels, steam generation in helical coils and in nuclear reactor cores) [27]. There are several recent experimental studies on flow boiling effects of nanofluids with significant consequences for enhancing boiling heat transfer. Boudouh et al.[20]. Found that the local heat flux, vapour volume fraction and heat transfer coefficient increase with increasing nanoparticle concentration and varying axial location when he studied boiling heat transfer and pressure drop through a rectangular channel of nanofluid. Another experimental study was directed by Lee and Mudawar [21] to discover the benefits of spreading (Al_2O_3) nanoparticles in water for microchannel-cooling applications. They found improvement of the heat-transfer coefficient for single-phase laminar flow; however, in the two-phase regime, the nanoparticles settle and form large agglomerations in the fluid, which can block the entire microchannel. This clogging problem is a serious issue if nanofluids are to be incorporated in microchannel cooling of microelectronics components, where any temperature excursions can result in temperature hot spots and possible thermal failure of the device. Xu and Xu [28] studied Al_2O_3/H_2O (0.2 wt.% concentration, 40 nm nanoparticle diameter) nanofluid flow boiling in a micro-channel (0.1 mm × 0.25 mm). The heat transfer was enhanced and they provided the bubble departure frequency is greater and the bubble contact angle is smaller in nanofluid. Based on the theory of nanofluids, the concept of nano-refrigerants has been projected. Studies on nano-refrigerants ([7], [19], [29], [30], [31], [32]) have shown that adding nanoparticles to refrigerants can improve the heat transfer

coefficient of the base fluid. Simultaneously, energy conservation and emission reduction are achieved. Henderson et al. [19] studied the flow-boiling heat transfer of R-134a-based nanofluids in a horizontal tube and found that the nanofluid has an insignificant influence on the flow pressure drop compared to the base fluid and that the heat transfer coefficient increases to double over the base-fluid. Sun and Yang [32] investigated the flow boiling of nano-refrigerants (Cu/R141b, Al/R141b, Al_2O_3/R141b, and CuO/R141b) in a horizontal channel with 10 mm inner diameter. They presented that the heat transfer of nano-refrigerants are increased with increasing mass fraction, quality and velocity.

CHF improvement during forced convection of flow boiling of a nanofluid on a short heated surface is experimentally studied by Ahn et al. [22]. They found that the nanofluid flow boiling heat transfer is enhanced under forced convection and they suggest that this enhancement is mostly caused by the nanoparticles depositing on the heater surface during boiling. Kim et al. [25] studied subcooled flow boiling (boiling adjacent to a surface hotter than the saturation temperature (T_s), whilst the bulk temperature of the local fluid is below T_s) using different types of nanofluid. They found that the heat transfer coefficient of the nanofluid increases during boiling and that the flow boiling critical heat flux (CHF) (point at which transition from nucleate to film boiling occurs) was enhanced using nanoparticles. Kim et al. studied another case [33] by investigating the enhancement of CHF for alumina nanoparticle based nanofluid in water at low pressure. They found that the CHF can improve up to 30% with 0.01 vol. % of alumina nanoparticles. [34] reported that the CHF increased more, as the higher pH levels (up to 12.3) of SiO_2 nanoparticles–water nanofluids, relatively little influence on the nucleate boiling regime. [35] stated that the CHF in water based Al_2O_3 nanofluids is improved by up to 51% compared to pure water but the boiling heat transfer coefficient is considerably degraded. They theorised that the reasonable effect for the changes in boiling heat transfer performance was the nanoparticle deposition onto the surface, which was confirmed by the surface roughness measurement after nanofluid boiling tests and the consequent change in nucleate site density.

Not all studies confirm the enhancement of boiling heat transfer as the nanoparticles concentration increases. For nucleate boiling, the heat transfer coefficient was sometimes decreased [36], [37], unaffected [18], [38], rather than increase by nanoparticles as mentioned before. For example, Abedini et al. [39] investigated experimentally a comparison of nanofluid flow boiling in vertical and horizontal tubes. They found that the subcooled flow boiling decreases with increasing concentration of TiO_2 nanoparticles in water. They also found that the bulk temperature decreases at the end of the channel in the nanofluid compared to water, implying that the vapour volume fraction increases in the nanofluid because of enhancing in the heat flux as the nanoparticles concentration increase. Witharana [40] in 2003 confirmed experimentally that the boiling heat transfer coefficient behaviour of the nanofluid depends on the type of nanoparticles, where Au (0.001 wt. %)-water nanofluid showed a clear enhancement in the heat transfer coefficient but SiO_2 (0.04 wt. %)-water and SiO_2 (0.025 wt. %)-ethylene glycol (EG) showed weakening of the heat transfer coefficient. These results imply that careful consideration of nanoparticle to base fluid is necessary to enhance heat transfer.

Although other studies investigate the effect of concentration of nanoparticles on heat transfer or critical heat flux in both pool and flow boiling [19, 24, 41-44], it is not done for salt nano-fluids. Likewise, there are many studies related to the flow pressure drop across a heating section [20, 21, 23], but no study is found related to the effect of nanoparticles on the overall pressure of the boiling system, i.e. on the saturation pressure of the solution. In this work, the properties of the nano-salt-fluid (acetone / $ZnBr_2$ (basefluid) – Graphene (nanoparticles)) are investigated. The acetone / $ZnBr_2$ chosen due to the low temperature operations (the process of separating two fluid vapours from each other) in VARS comparing to other working fluid [45, 46]. The effects of the nanoparticle concentration (0, 0.1, 0.2, 0.3, 0.4, 0.5 vol. %), the boiler temperature (411, 418, 426, 436 and 446 K) and the flow rate of the nanofluid in the boiler (2.3, 3.66, 4.2 and 7.1 ml/s) on the heat transfer, saturation temperature of the solution, temperature of the fluid, saturation temperature, concentration of the salt in the strong solution reservoir (SSR) and condenser flow rate are investigated. This study gives a better understanding for the behaviour of the salt nanofluid flow boiling in the rectangular duct which represents the boiler in a VARS.

Experiments

1- Preparation of nano-salt-fluid

Acetone / $ZnBr_2$ with 50 wt. % $ZnBr_2$ was prepared by dissolving 500 g of $ZnBr_2$ into 500 g of acetone which made 0.734 L of solution producing the measured density 1362 kg /m^3. With this solution the effects of boiler temperature and flow rate were investigated on the solution without nanoparticles. After each test, acetone was used to flush the rig in case some salts or nanoparticles stuck in the pipes or joints. A further identical sample of acetone / $ZnBr_2$ was prepared for addition of nanoparticles using the two step method, which was then tested in the same way as the base fluid.

According to the density of Graphene ((catalog Number:06−0210/25g) were purchased from Strem chemical, Ltd. Company), 1800 kg/m^3 with 6-8 nm thickness and 5 μm width and the volume fraction required for 0.1 vol. %, 1.32 g of nanoparticles is required.

The solution is sonicated (ultrasonic excitation) before each test with a sonication probe (Cole-Parmer 750 Watt Ultrasonic homogenizer) using 45% of the maximum amplitude for 30 minutes to break the particle agglomerations. The proper sonication time was found in a separate test performed with four samples with different times of sonication (without sonication, 30 mins, 1hour and 2hours). The sonication for 30 minutes was chosen for two reasons: firstly, the stability of the sample with 30 minutes sonication is better than the sample without sonication and it does not differ significantly from the one hour and two hours sonication samples. Secondly, with longer time of sonication the solution becomes warm and a part of the acetone evaporates from the solution. The stability of a nanofluid is a key issue. Graphene in acetone / 50 wt. % $ZnBr_2$ shows a good stability for 4 hours as shown in Figure 1, then the particles commence sedimentation (during the circulation of the fluid in the rig the nanoparticles remain suspended for an even longer time). The stability of this solution is affected by the density of the basefluid which depends on the concentration of the $ZnBr_2$; by making the salt ($ZnBr_2$) concentration 60 wt. % the nanofluid stays stable for 30 hours. But in this experiment, the 50 wt. % salt concentration is important because it effects on the viscosity

in the strong solution reservoir of the VARS, which would turn cause crystals to form in the process vessels. The duration of sonication beyond 30 min shows insignificant change in the stability. Therefore, 30 min sonication was chosen.

To analyse the distribution of the particles in the fluid, after the sonication, the sample was imaged with Transmission Electron Microscope (TEM). The samples for TEM were prepared by casting several drops of the sample solution onto copper-mesh holey-carbon film TEM grids (Holey Carbon support films (HC range), and samples are dried under ambient conditions). Figure 2 shows the graphene on the carbon film. Figure 2a shows the graphene particles on both film. The particles appear in a different levels of shading between grey and black because of the thickness of the particles, which caused by the agglomeration. Whereas the thick part of the body makes a black trace because the thick part prevent the electrons stream to pass through it and most of these electrons scattered in the high angles. While, the

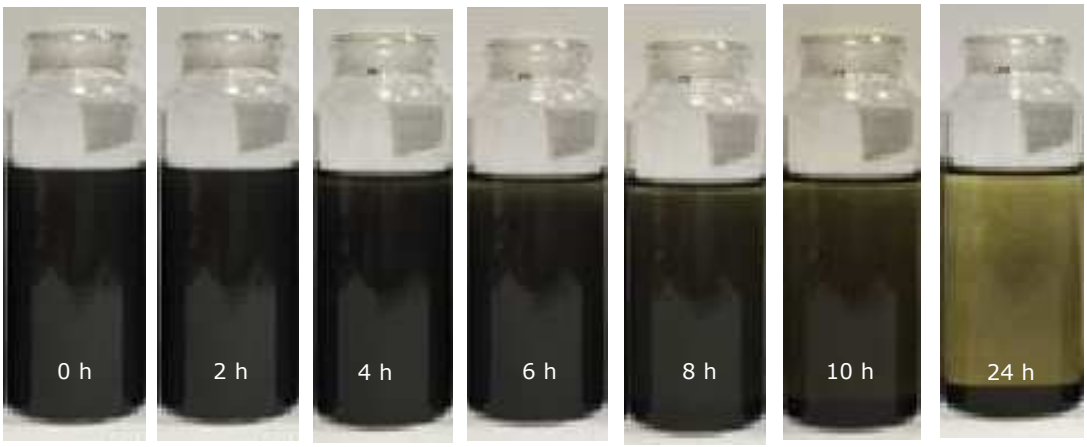

Figure 1: Sample of acetone /$ZnBr_2$ (50 wt.% $ZnBr_2$) with 0.1 vol. % Graphene. After sonication for 30 minutes, shows stability till 4 hours.

grey colour means a thin part of the body, which allows most of the electrons to pass. Figure 2b shows a bodies of graphene stuck on the carbon film and the shading levels also mean overlapping several particles. Figure 2c shows a crystallising of $ZnBr_2$ appears in a black colour also it shows a single particle stuck on the carbon film. From figure 2d, it can recognised that there are some grains of the $ZnBr_2$, which have very small size (around 1 nm).

2- Properties of the solutions

The properties of the working fluid were measured for different concentrations of nanoparticles. The density of the pure acetone / $ZnBr_2$ (50 wt. % $ZnBr_2$) was found equal to 1360 kg/m^3, however in the [47] is 1581 kg/m^3. Also different concentrations of $ZnBr_2$ were investigated which all gave a significant difference. The possible explanation for this difference is that [47] may assume that when the salt ($ZnBr_2$) is added and dissolved in the acetone, the volume of the acetone is not changed. The volumetric flask used in this measurement was with the narrow neck, which reduce the errors. The fluid level on the flask's mark may have an error of ±0.5 mm and the diameter of the neck of flask is 10 mm, which makes the error range on volume (±0.4%) for the 10 ml prepared solution. Regarding the nanofluid, the experimental results compared well with a simple mixture combination method in Equation 1 showing a good agreement as shown in Figure 3a.

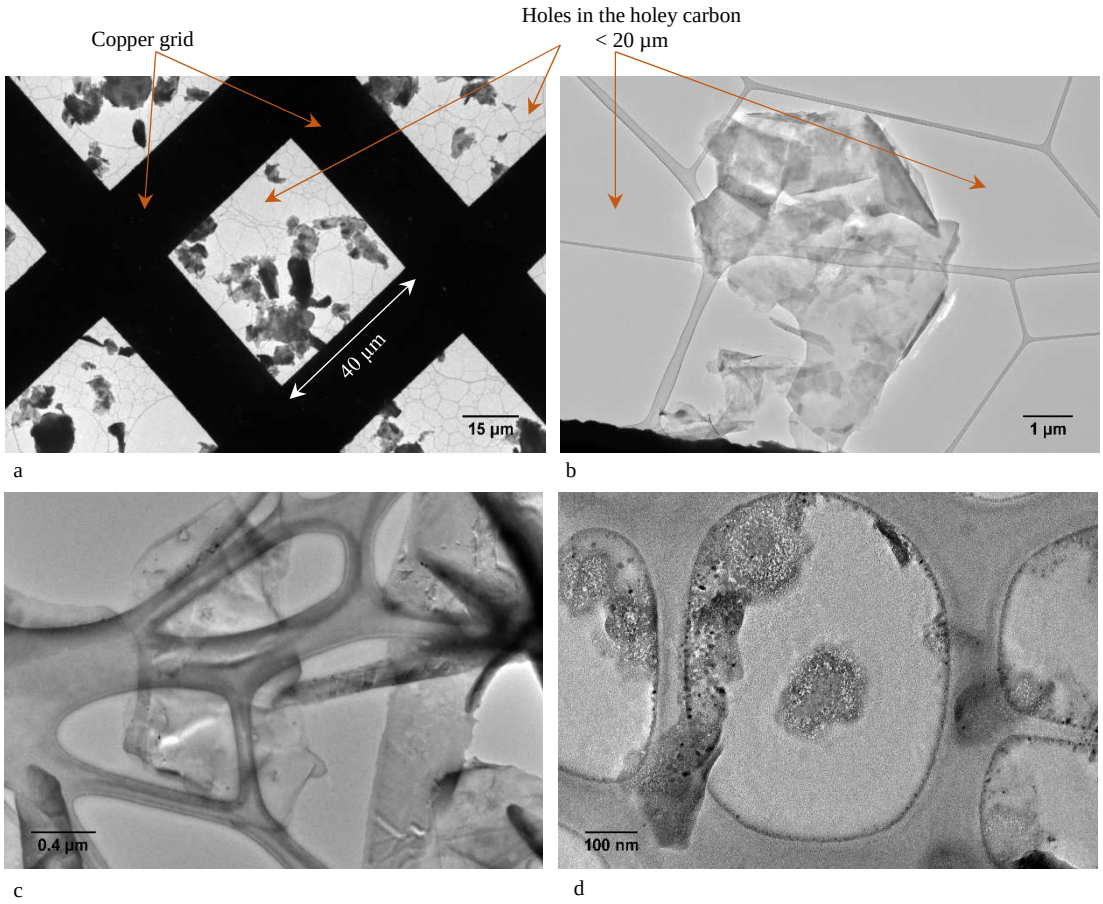

Figure 2: Different TEM images of graphene suspend in the acetone / $ZnBr_2$ on the Copper mesh holey Carbon film.

$$\rho_{nf} = (1 - \varphi_p)\rho_f + \varphi_p\rho_p \quad \text{Equation 1}$$

Where ρ and φ are the density and the volume fraction, and subscripts p, f and nf represent particles, base fluid and the nanofluid respectively. The density of the nanofluid increases with increasing concentration of nanoparticles, for example, the density increases from 1360 to 1362.7 kg/m^3 when the concentration increases from 0 to 0.5 vol. %. To get a better idea of the actual data of the density and characterize the uncertainty of these values, the measurement for each case was repeated five times in different sized containers. Figure 3a also, shows the mean uncertainty (Equation 2) (the actual value of x will be somewhere in a neighbourhood aroundx_{mean}. This neighborhood of values is the uncertainty in the mean) was found for each concentration measurement.

$$x_{mean} = \frac{x_{max} - x_{min}}{2\sqrt{N}} \quad \text{Equation 2}$$

Where x and N are the reading and the number of measurements respectively.

The thermal conductivity of the different concentrations of nanofluid were investigated using thermal conductivity analyser C-THERM TCI. The samples are sonicated for 30 minutes before measuring to ensure the distribution of nanoparticles in the fluid. The thermal

conductivity increases from 0.150 to 0.157 W/m.K when the concentration of the graphene nanoparticles increases from 0 to 0.5 vol. %, this means that the thermal conductivity increases by 4.5% by adding 0.5 vol. % of the nanoparticles to the solution. The experimental results have compatibility with the Suganthi model (Equation 3) [1] as shown in Figure 3b . The test is repeated 5 times for each sample and the uncertainty calculated in the same way as the density calculation (k is the thermal conductivity).

$$k_{nf} = k_f(1 + 7.926\varphi_p) \quad \text{Equation 3}$$

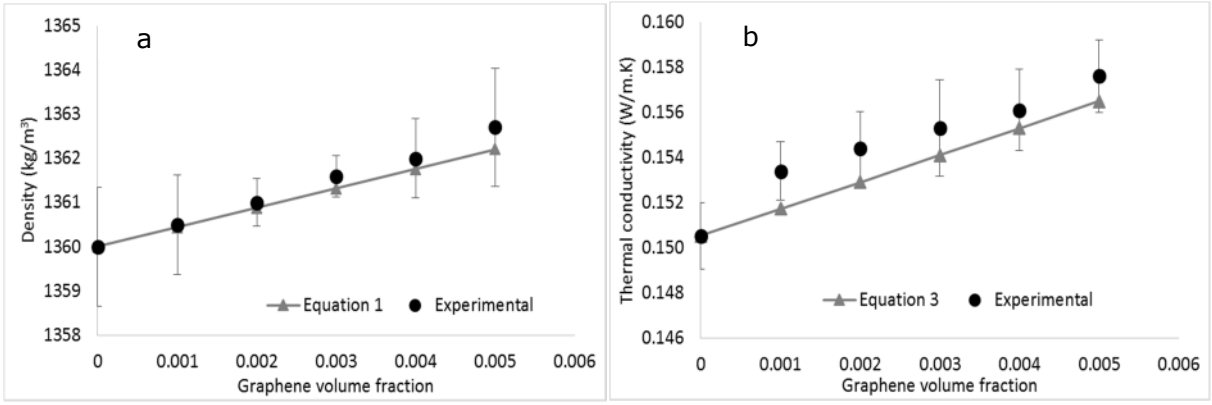

Figure 3: Effect of the nanoparticles on a) density and b) thermal conductivity of the acetone / $ZnBr_2$ (50 vol. % $ZnBr_2$) bars show the uncertainty of each reading.

The heat capacity of the nano-salt-solution was also investigated using TA instrument Q10 Differential Scanning Calorimetry DSC. Also, each test was repeated 5 times after sonication. The experimental heat capacity of the pure acetone / $ZnBr_2$ is 1.14 (J/kg.K) and it decrease to 1.131 (J/kg.K). The heat capacity reduces with increasing concentration of graphene. Also comparing the results with a simple mixture combination method (Equation 4) used by different researchers [48, 49], the experimental result shows a good agreement with the theoretical as shown in Figure 4a (c_p is the heat capacity).

$$c_{p\,nf} = (1 - \varphi_p)\rho c_{p\,f} + \varphi_p c_{p\,p} \quad \text{Equation 4}$$

There is evidence that particle type affects viscosity, but most derived correlations assume that only concentration is significant. The viscosity of the graphene nano-salt-fluid was derived from tests on ZnO in acetone zinc bromide solution nanofluid. A trendline equation of the ZnO nanofluid (Equation 5) (μ is the viscosity) was obtained using an hts-VROC viscometer rheometer on a chip. No further measurements were available on viscosity of nanofluids in this work, and the graphene nanofluid viscosity was therefore assumed from the similar ZnO nanofluid in the same base fluid over the lower range of particle concentrations tested. The viscosity of acetone found as 0.308±0.007 mPa.s using both Equation 2 and Equation 5. The concentrations of the ZnO used in the same acetone /$ZnBr_2$ (50 wt. % $ZnBr_2$)

were between 0 - 1.2 vol. % and the maximum uncertainty was found at the concentration of 1.2, for which the viscosity is 4.79±0.4 m Pa.s.

$$\mu_{nf} = -6669.3\,\varphi^2 + 197.29\varphi + 3.32 \qquad \text{Equation 5}$$

Figure 4b shows how the viscosity of the Graphene nanofluid increases with increasing concentration of nanoparticles according to Equation 5. Viscosity is significant for the power needed to pump the solution to the rig circulation.

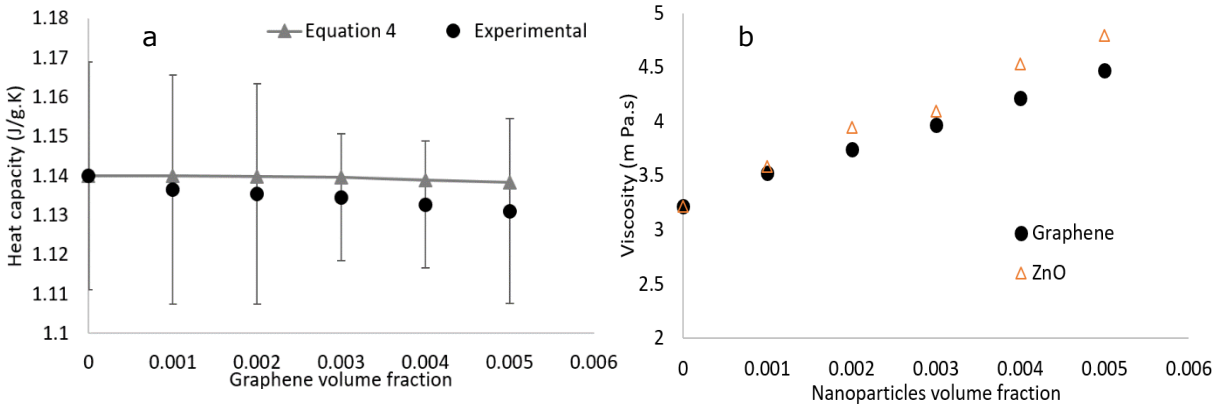

Figure 4: Effect of the nanoparticles on a) heat capacity and b) viscosity of the acetone / $ZnBr_2$ (50 vol. % $ZnBr_2$). Bars show uncertainty of each reading for Figure a.

3- Flow boiler experimental setup and procedure:

In the test rig, shown schematically in Figure 5 a consists of 1 L weak solution reservoir (WSR), supplies an R400BL conical revolution micropump and flow rate controller (made by TCS Micropumps Company) which transports the weak solution (WS) from the WSR to the boiler via an EPDM rubber tube, which is chemically compatible with the acetone/$ZnBr_2$ solution. The boiler in **Error! Reference source not found.** has a 250 W strip heater (15 cm length, 1.5 cm high and 3.6 cm wide) fixed to flat plate heat exchanger and has 5 K-type thermocouples separated by 3 cm distance between them. The temperature of the boiler is controlled via a PID controller (Omega CSi8D series). The strong solution (SS) with the acetone vapour (refrigerant) pass to the strong solution reservoir (SSR) with Dreschel bottle on top to separate the refrigerant, (ie acetone vapour) from the SS. The refrigerant enters the condenser (Liebig condenser) cooled by tap water (flow rate =26 g/s) and then the refrigerant reservoir (RR). Both the refrigerant and the SSR are terminated by valves at the base. The ends of the last two reservoirs are connected with the WSR using a three way adapted tube.

After preparing the working fluid, it is loaded to the WSR, the pump is activated to measure the flow rate of the system by collecting the solution in the SSR for several volume levels indicated on the flask. The flow rate is controlled via a potentiometer on the controller. Once the flow rate is achieved, the boiler heater element is activated at the desired temperature using the PID controller.

The solution passes through the pump from the WSR to the boiler, where it boils. Acetone vapour (refrigerant) is produced, then both the solution and the refrigerant are collected in the SSR. The refrigerant fills all the empty space in the SSR, expands and expels any air in the rig to the condenser and the refrigerant reservoir (RR). By increasing the vapour in the rig, the pressure increases. Due to non-condensable air in the system, the refrigerant can't condense in the condenser. To extract the air, the join between the condenser and the RR is opened and closed quickly when the pressure reaches 1.3 bar. The pressure decreases, and by generating more vapour it increases again to 1.3 bar, the join is opened and closed again to expel more air. At the third time all the air is expelled as shown in Figure 7. The condenser then (after 1100 s from the system operations) starts to condense the refrigerant, see **Error!**

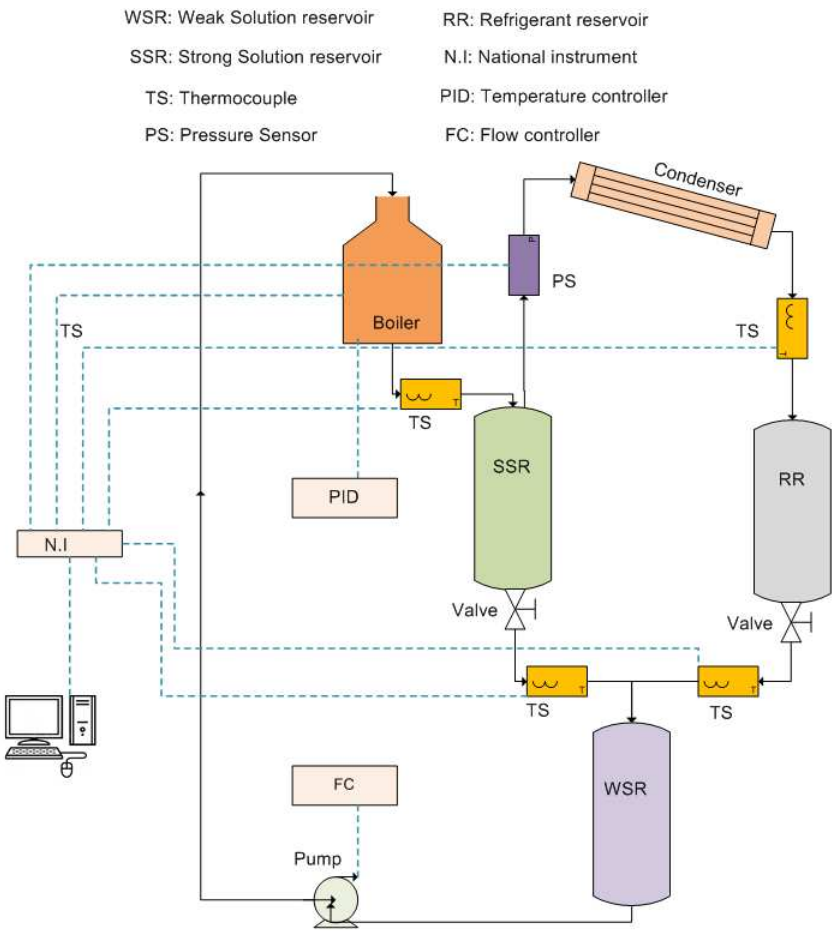

Figure 5: Equipment schematic of the high pressure side of the VARS. Weak solution reservoir (WSR) delivers the weak solution (WS) to the pump, controlled by the flow controller (FC). The pump supplies the boiler heated by 15 cm x 3.6 cm strip heater (250 W). The strong solution and the acetone vapour separate in the strong solution reservoir (SSR). The vapour condense in a Liebig condenser then collected in the refrigerant reservoir (RR). The SSR and RR outflows converged in the WSR. Completing the cycle.

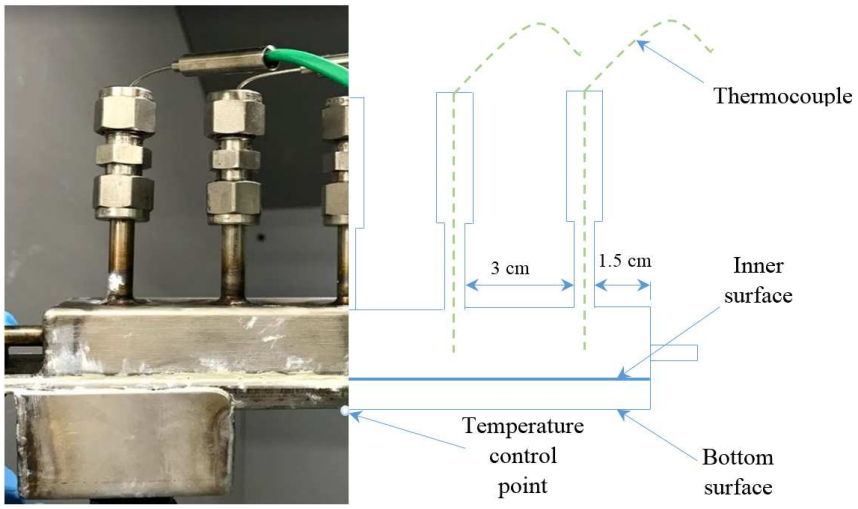

Figure 6: Strip heater (boiler) used in this experiment. Type Caloritech, 250 W.

Reference source not found.. The temperature of the flow in the condenser rapidly increases to the saturation temperature (60°C). The absolute pressure of the system stabilizes when the condensation and the boiling rates are equal. The condensing rate is calculated by measuring the flow rate of the refrigerant which collects in the RR. Both the SS and the refrigerant mix again in the three-way pipe junction to produce a WS collected in the WSR (completing the cycle) then the process is continued.

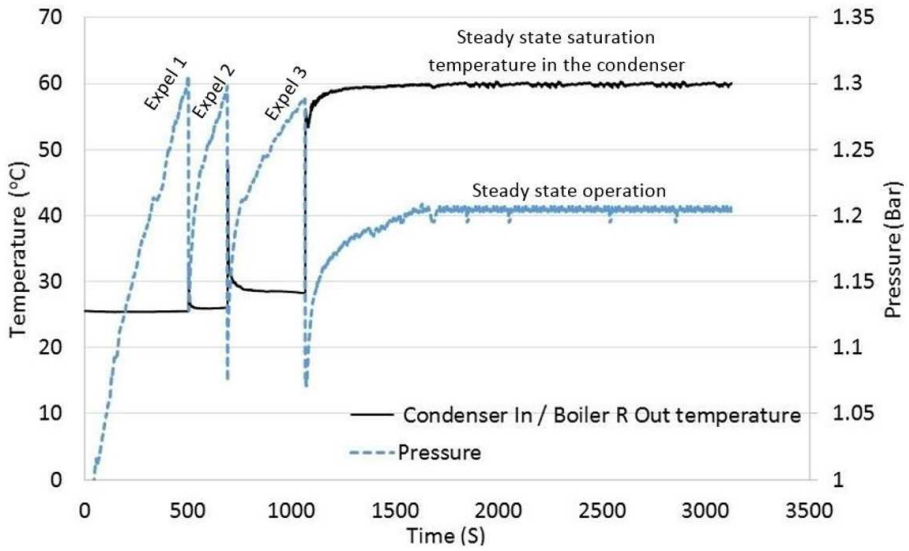

Figure 7: The temperature of the condenser and the absolute pressure of the system as a function of time. In case (flow rate 3.6 ml/s, 426 K and 0 concentration of nanoparticles).

4- Calculation and measurement of the parameters:

To analyse the outcome from the experiment, the following parameters are investigated: heat flux, heat transfer coefficient, Rohsenow correlation constant and the concentration of the salt and the nanoparticles in the solution.

Flow boiling heat transfer is complicated and difficult to correlate as it depends on two effects, the bubble creation with the flow near the hot surface and sweeping of heater by the liquid. There are no general correlations for flow boiling data. The heat transfer rate combines from both nucleate boiling and forced convection phenomena [50]. As described in Equation 6

$$q'' = q''_w + q''_c \quad \text{Equation 6}$$

Where q''_w is the nucleate boiling, q''_c is single phase convection boiling.

The most important part of a boiling process is nucleate regime boiling. The heat flux can be estimated using the earliest and most successful correlation used by many researchers such as [51] and [52]. This correlation was developed by Rohsenow and it applies for clean surfaces and depends mainly on the properties of the fluid as well as a constant for surface-fluid interaction (C_{sf}). The Rohsenow nucleate boiling correlation is

$$q''_w = \mu_l h_{fg} \left[\frac{g(\rho_l - \rho_v)}{\sigma}\right]^{0.5} \left[\frac{c_{p,l}(T_w - T_{sat})}{Pr_l C_{sf} H_{fg}}\right]^3 \quad \text{Equation 7}$$

Where μ is the liquid phase viscosity (3.23 mpa.s (measured)), h_{fg} is the latent heat for acetone (518 kJ/kg [53]), ρ_l is the liquid density (1360 kg/m^3 (measured)), ρ_v is the acetone vapour density (0.824 kg/m^3 [54]), σ is the surface tension between liquid and surface (0.024 N/m [55]), $c_{p,l}$ is the heat capacity of the liquid (1140 J/kg.K (measured)), the thermal conductivity to measure the Prandtl number (Pr) is 0.152 W/K.m (measured), C_{sf} Rohsenow constant (dimensionless), H_{fg} enthalpy(106.4 kJ/kg) [56]).

During the tests conducted over several hours, there was no evidence of particle deposition in the boiler channel as verified by flushing the system with pure acetone at the end of each campaign. The flushing acetone emerged clear indicating that there was no deposited nanoparticles, and no deposited salt on the walls of the boiler. Therefore, there is no anticipation for the nanofluid and the nucleate boiling regime tested, that there will be any significant deposition, which effect on Rohsenow constant. The C_{sf} of acetone / $ZnBr_2$ on the stainless steel (boiler metal) is unknown. We found the C_{sf} depending on the Equation 7 using the electricity power input, which equals 48.8 W (the average power consume by the boiler as the PID controller switching the power between on and off to control the temperature) for all the cases (different flow rate and different wall temperature) and the average C_{sf} was calculated. The C_{sf} is dependent on the surface temperature. In the case of studying the effect of the nanoparticles and the flow rate, the boiler temperature is constant (426 k) which has C_{sf} equal to 0.217. However, in the boiler temperature variation test, the average of 0.217 is between the maximum and the minimum, which is a reasonable first analysis for heat flux calculation. In single component fluid boiling, the properties of the liquid remain constant; in

the salt solution, as the boiling temperature increases, the concentration of the solution increases and some effect will therefore be experienced as noted in Table (1).

The single phase heat flux q_c'' could found by

$$q_c'' = h_c\,(T_w - T_m) \quad \text{Equation 8}$$

$$h_c = \frac{Nu\,k}{D} \quad \text{Equation 9}$$

$$\text{Nu} = 0.019\,Re^{4/5}pr^{0.4} \quad \text{Equation 10}$$

Table 1 the values of the C_{sf} at different flow rate and wall temperature.

Flow Rate (ml/s), at 426K wall temperature	C_{sf}	**Wall Temperature (K), at 3.66 ml/s flow rate**	C_{sf}
2.31	**0.211**	**411**	**0.177**
3.35	**0.217**	**418**	**0.198**
3.66	**0.215**	**426**	**0.217**
4.27	**0.220**	**436**	**0.239**
7.1	**0.222**	**446**	**0.255**
Average	**0.217**	**Average**	**0.217**
Total average		**0.217**	

5- Error analysis

The thermocouple uncertainty is stated as ±2.5 ^{o}C and pressure transducers ±0.04% of the scale (makes the maximum error in the pressure 3 bar * 0.0004 = ±0.0012 bar) [57]. The tolerance in the thermocouples affects directly on the calculations of the heat flux then the heat transfer coefficient. The heater temperature fluctuated, e.g. when the controller was set on 426 K, the temperature of the heater fluctuated between 424 K and 432 K. The rig was not insulated and heat loss was likely in some sections i.e. losses from the wall of the heater, walls of WSR, walls of SSR and the tubes.

Preparation of the nanofluid causes some errors during weighing and checking their volume. Another source of error is measuring the properties of the solution. There are some random errors which cannot controlled such as:

- Changing the properties of the solution by changing the laboratory temperature during the test. The temperature of the first day of the test was 23 ^{o}C and it fluctuated between

20 and 26 °C and this will effect on the properties of the solution and heat loss to the environment.

- ❖ Some salts and nanoparticles deposited on the walls of the rig (in the joins and the tubes) which affects concentration of the $ZnBr_2$ and nanoparticles in the solution.
- ❖ Some acetone vapour may escape from the rig during the ventilation (opening the joint between the condenser and the RR to extract air from the rig).
- ❖ Some acetone vapour condensed on the wall of the SSR. So, not all the vapour generated in the boiler condensed in the condenser.

The flow rate variation was checked for one case for the basefluid with temperature (426 K) repeated 5 times, and the volumetric flow rate showed a small difference in each time. The other parameters uncertainty of the mean value for each parameter calculated depending on Equation 11:

$$Uncertainty = \frac{X_{max} - X_{min}}{2\sqrt{Average}} \quad \text{Equation 11}$$

The measured values and the uncertainties calculated are in acceptable range which was 3.685 ± 0.040 ml/s for the flow rate and 8703.89 ± 85.14 W/m^2, the data are shown in table (2) where q'' calculated through Equation 7 and U is the overall heat transfer coefficient calculated via Equation 12

$$q'' = U\,(T_w - T_m) \qquad \text{Equation 12}$$

Table 2: shows the measured values with the uncertainty for data measured and calculated for 5 trails for one case for pure acetone / $ZnBr_2$ solution and controlled temperature =426 K.

Parameters	1st trial	2nd trial	3rd trial	4th trial	5th trial	average	Measured value
Flow rate (ml/s)	3.57	3.61	3.66	3.70	3.75	3.66	3.685±0.04
q'' (W/m^2)	8558	8618	8653	8745	8939	8702	8703±85
U (W/m^2.K)	103.11	103.59	103.87	104.11	105.17	103.97	103.96±0.46
T_{mean} (K)	343	342.80	342.69	342	341	342.30	342.29±0.44
T_{sat} (K)	335.3	335.1	335	334.7	334	334.82	334.82±0.29
Cond. Flow (ml/s)	0.075	0.076	0.077157	0.0785	0.08	0.077331	0.0773±0.0011

Discussion

1- Effect of the concentration of Nanoparticles at constant flow rate and boiler temperature.

In this part of the work, the effects of increasing nanoparticles in the base fluid on the system pressure, heat transfer, heat transfer coefficient, saturation temperature of the system, average boiler temperature and the condenser flow rate are studied. The concentrations used are 0.1, 0.2, 0.3, 0.4 and 0.5 vol. % with a constant flow rate and temperature of the lower surface of the boiler of 3.63 ml/s and 426 K, respectively.

Figure 8a shows that the steady state boiling pressure increase from 1.13 bar to 1.24 bar when the concentration increases from 0.1 % to 0.4 %. Increase in the nanoparticle concentration will increase the heat transfer and the thermal conductivity of the fluid, which helps generate more vapour from the boiler. The line of the highest concentration (0.5 vol. %) cuts out at 2550 (s) because it caused repeated failure of the pump on three separate occasions, most likely due to an increase in pump operating temperature which in turn is likely connected to the increased boiling temperature and therefore general rise in system operation temperature. Because the pressure is affected by nanoparticle concentration, the saturation temperature at the condenser side for pure acetone is also affected as shown in Figure 8b, increasing according to the increase saturation pressures.

Figure 9 illustrates heat transfer coefficient and heat flux (calculated via Equations 6-10) tending to increase as the concentration of the nanoparticles increases. The particles assist heat transfer from the surface into the liquid. Heat flux and heat transfer coefficient increase from 104 W / m^2. K and 8.65 kW / m^2 to 167 W / m^2. K and 13.16 kW / m^2, respectively, when the particle loading rises from 0 vol. % to 0.5 vol. %. The thermal conductivity of the nanofluid is enhanced with increasing the nanoparticles. Despite the thermal diffusivity being greater than Brownian diffusivity of nanoparticles in the liquid [58, 59], nano-particles undergo inter-particle collisions, and thermal interactions with molecules of the fluid and with the surface of the heater and these effects compound to increase the heat transfer [60, 61].

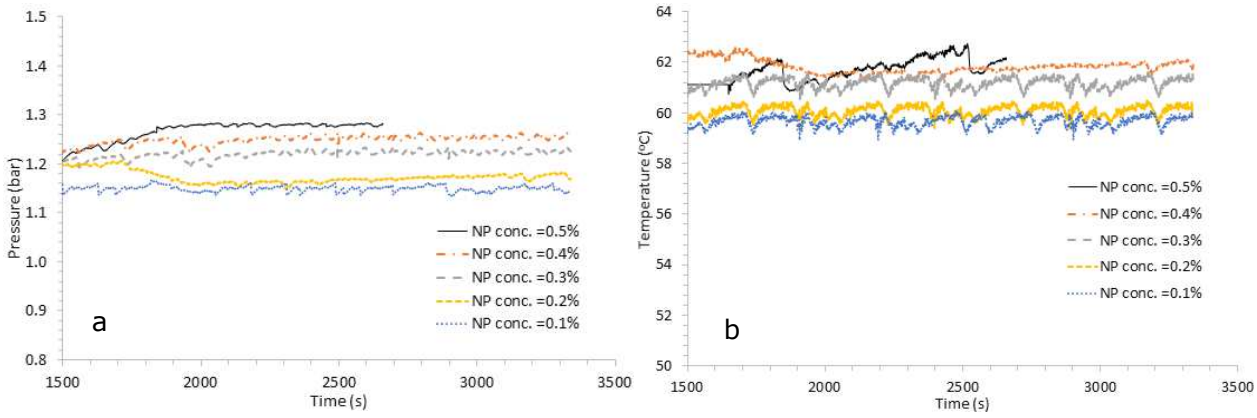

Figure 8: Steady state regions the a- pressure b- saturation temperature of the pure acetone at different concentration of nanoparticles in VARS.

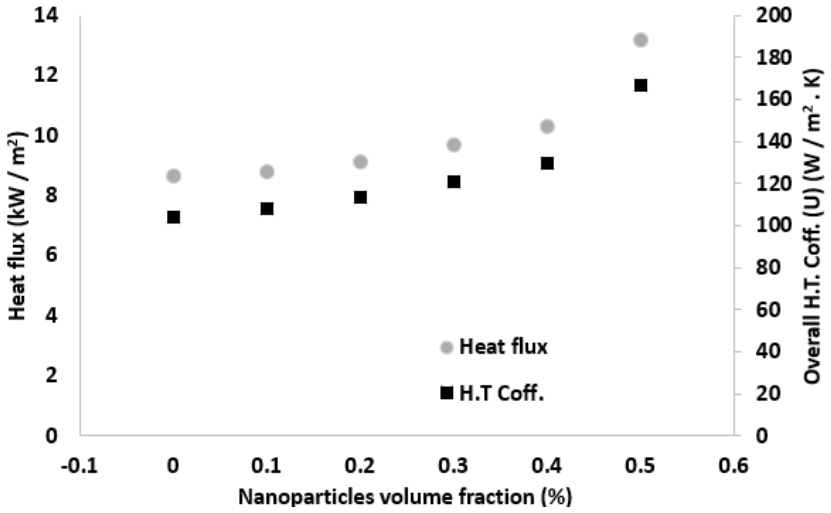

Figure 9: Relationship between the heat flux and the overall heat transfer coefficient in the boiler with the different concentration of nanoparticles in VARS.

Figure 10 shows that increasing the concentration of the nanoparticles from 0 to 0.5% vol. raises the average boiling temperature from 342.7 K to 347 K. The saturation temperature of the acetone over the strong solution increases from 332.7 K to 335 K as shown in Figure 10a. Heat flux in **Figure 9** increases due to increased thermal conductivity; the condensation rate increases around 3.6 times as shown in Figure 10b; the salt concentration in the SSR increases as more acetone leaves the solution; the concentration of the nanoparticles increase in the SSR. The enhanced heat flux seen in Figure 9 gives rise to improved nucleate boiling, and therefore a greater yield of acetone; this in turn raises the concentration of the solution in contact with the vapour in the SSR; that is what causes the increase of the acetone saturation pressure and temperature since the mass transfer driving potential for acetone absorption is the concentration of the salt solution, which attracts the vapour back into the solution in competition with the condenser.

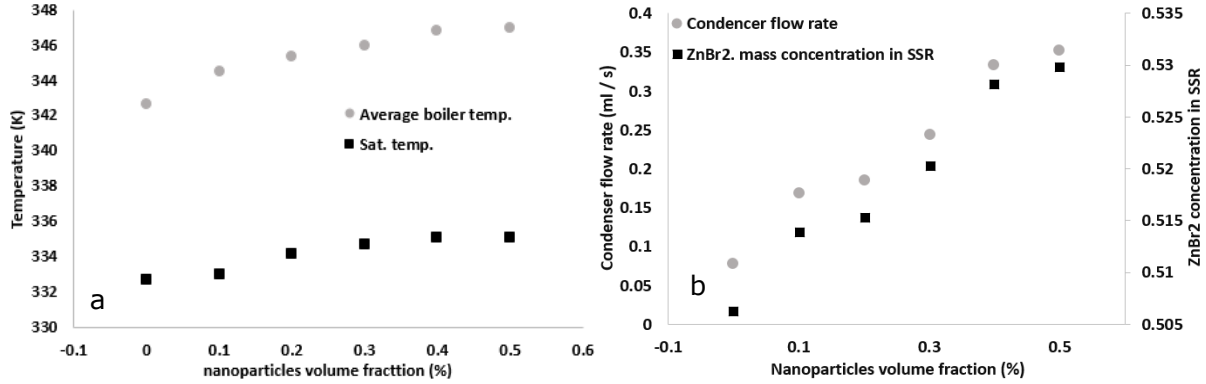

Figure 10 a- Relationship between the saturation temperature of acetone in the condenser and the average boiler temperature with the different concentration of nanoparticles. b- Relationship between the $ZnBr_2$ concentration in SSR and the condensed acetone flow rate in the condenser with the different concentration of nanoparticles.

Many studies include the effects of the surface temperature on the parameters [6, 13, 22, 36, 62-66]. In this study the effect of the wall temperature is investigated for the basefluid (slat solution without nanoparticles) because the similarity of the behaviour between the basefluid and nanofluid. 5 different surface temperatures, 411, 418, 426, 436 & 446 K, were studied their effects on the boiling of the salt solution at the constant flow rate (3.35 ml/s). The saturation temperature of acetone in the salt solution with 50 wt. % $ZnBr_2$ under atmospheric pressure and the saturation temperature of pure acetone are 340 K and 330 K [47], respectively, and they increase with increasing the pressure of the system.

Increasing boiler surface temperature increases the pressure generated in the system as shown in Figure 11a, e.g. at 411 K the pressure is 1.16 bar and at 446 K the pressure stabilized at 1.39 bar. With increasing heated surface temperature, the time to stabilize decreases (when the condensing rate is equal to the boiling rate). At 411 K, the pressure stabilized after 40 minutes, however, it is stabilized in 25 minutes for 446 K case. At higher temperature, the salt solution vapour pressure increases producing a higher system pressure. The saturation temperature of the pure acetone is less than the boiling point of the salt solution [47].

Figure 11b shows how the saturation temperature of the pure acetone, measured in the entrance of the condenser, increases with increasing temperature of the boiler. Increasing the boiler temperature will increase the vapour pressure of the system and consequently increases the saturation temperature of the acetone in the condenser. The points on each of the curves mean that the acetone starts to condense, and these points also show that the acetone condenses faster with a higher boiler temperature. The condensing process starts before stabilising the pressure for example in case of 411 K the condensing starts at 28 minutes, however, at 446 K it starts at 10 minutes. This behaviour happen because with lower temperature, less vapour generates which takes longer time to replace with the cold air in the system, which is necessary to extract to start the condensation process. However, with higher temperature more vapour generates, the pressure increase quickly, and when the joint between the evaporator and the condenser opened (as mention in section 3 (Flow boiler experimental setup and procedure)) each time, a sufficient cold air extract, which help to rev the condensation process.

The average temperature of the vapour/liquid mixture leaving the boiler also depends on the boiler temperature. Because the volume fraction of vapour is the majority phase by volume at exit from the boiler, and the vapour in the boiler cannot exceed the saturation temperature, then the temperature of the mixture at SSR is between 343 K and 349 K depending on the pressure, but the liquid temperature will be higher, which was not measured in this study.

Many studies such as [6, 13, 36, 62, 63] show that the relationship between the heat flux and the temperature difference between the wall and the saturation ($\Delta T_{sat.}$) is linear. However, a linear relationship but with two gradients; a slight initial slope, then the gradient increases has been reported [22] . Another study [66] found an exponential relationship between the heat flux and $\Delta T_{sat.}$. This relation appears because, by increasing ΔT_{sat}, transient and film boiling take over, which decrease the rate of heat flux. In our study the ΔT_{sat} was between 102 ^{o}C and 135 ^{o}C and the overall heat transfer coefficient (U) increase approximately linearly but the heat flux (q''_w) reflects a quadratic increasing with increasing $\Delta T_{sat.}$, suggesting

that the process is in the nucleate boiling range. The gradient of both q''_w and U are different (Figure 12) because they depend on different ΔT_{sat} and ΔT_{mean} as described in Equations 6-12 by the boiling and forced convection contributions of the heat flux. By increasing the $\Delta T_{sat.}$ in our cases, the relation becomes quadratic according to the left side of the typical positive skew curve seen in heat flux vs. $\Delta T_{sat.}$ for flow boiling heat transfer indicating a condition well within the nucleate boiling regime.

The concentration of the salt rises in the SSR as the boiler temperature increases, but even at the highest boiler temperature (446 K), the mass fraction increases only from 0.5 to 0.512 as shown in Figure 13. It also shows how the condensed acetone flow rate in the condenser increases correspondingly.

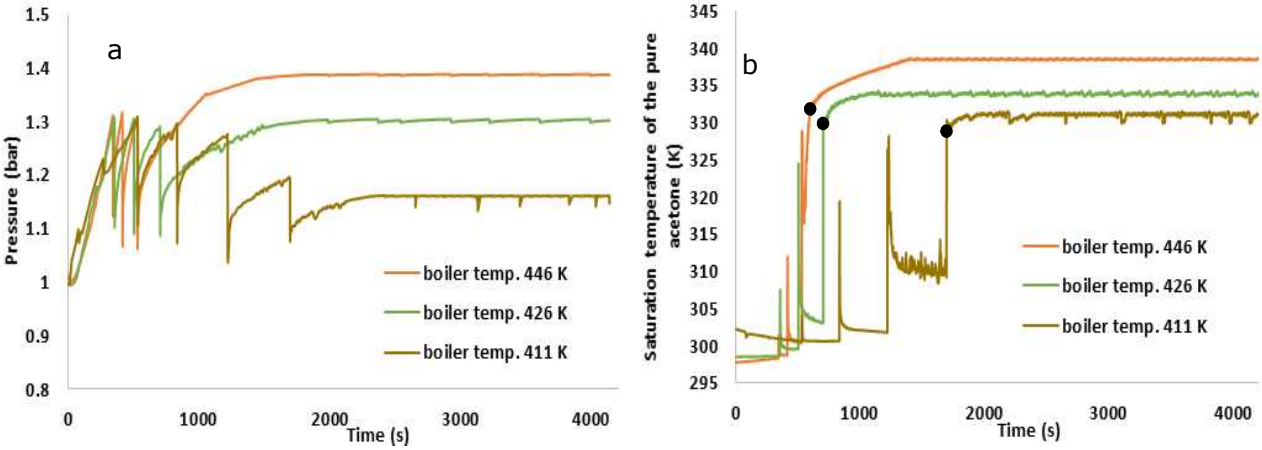

Figure 11: Developing the a- pressure b- saturation temperature of the pure acetone under the effects of the different temperatures.

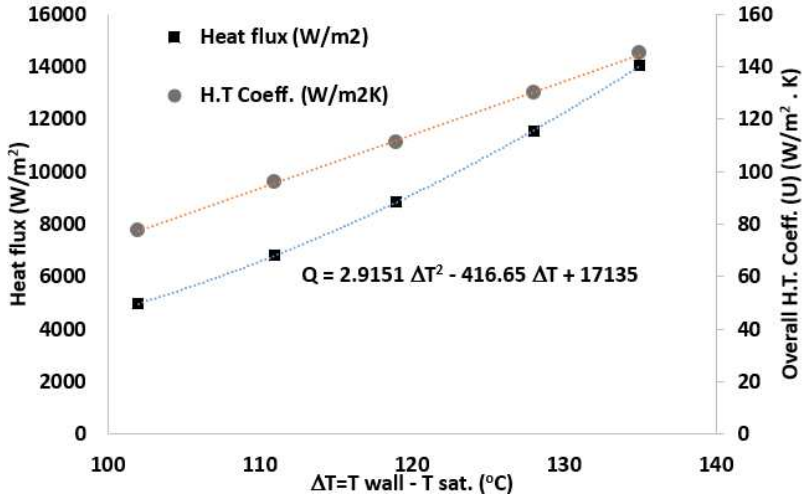

Figure 12: Relationship between the heat flux and the heat transfer coefficient in the boiler with the different the different $T_{wall} - T_{sat}$.

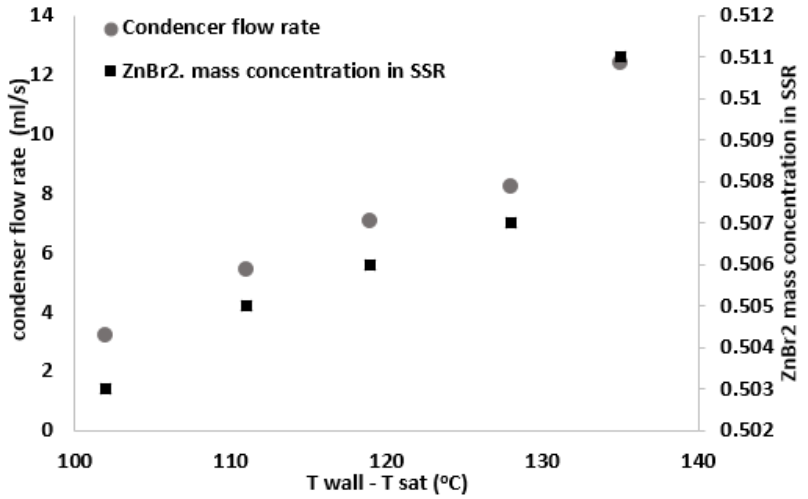

Figure 13: Relationship between the $ZnBr_2$ concentration in SSR and the condensed acetone flow rate in the condenser with the different $T_{wall} - T_{sat}$.

3- Effect of the flow rate of the basefluid at the constant boiler temperature.

The effects of the flow velocities on the boiling behaviour of the nanofluid was studied by different researchers [6, 22, 36, 67]. Four different flow rates, 2.31, 3.66, 4.27 and 7.1 ml/s, are investigated to determine the influence on heat transfer, temperature at the outlet, vapour generation in the boiler and the pressure of the system which in turn controls both the saturation temperature and the condensation rate in the condenser. At 2.31 ml/s, the pressure starts from the atmospheric and rises gradually to 1.2 bar which has a saturation temperature of the pure acetone of 60 ^oC and for the salty solution (50wt. %) is 74 ^oC [47].

Figure 14 shows that the heat flux and the heat transfer coefficient increase from 7878 W/m^2 and 93 $W/m^2.K$ to 9931 W/m^2 and 124.5 $W/m^2.K$ respectively when the flow increases from 2.31 to 7.1 ml/s. Heat transfer coefficient is the ratio of the heat transfer rate against the temperature difference across the surface layer and fluid boundary layer, and the heat capacity depends on the thermal conductivity of the boundary layer and its thickness only. Changing the velocity can influence the surface temperature and the measured liquid bulk temperature. The velocity might change (i.e. decrease) the thickness of this stagnant vapour layer where heat transfer is conductive. As a result the heat transfer coefficient increases. There is also increase due to convection in the fluid (heat sink) just above the boundary layer which is induced by the motion.

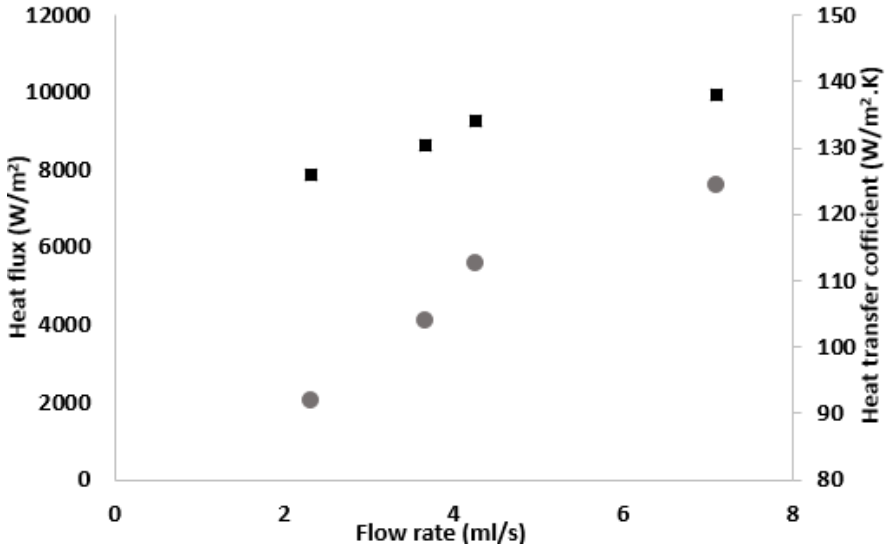

Figure 14: Relationship between the heat flux and the heat transfer coefficient in the boiler with the different flow rate.

When the fluid enters the boiler, its temperature increases as it flows. The temperatures are measured by five thermocouples which extend to the middle of the channel as shown in **Error! Reference source not found.**. The vapour volume fraction increases during the flow, and at the outlet of the boiler the vapour volume fraction can be more than 90% depending on the case. Evaporating the acetone in the boiler makes the concentration of the salt ($ZnBr_2$) increase in the SSR.

The average boiler exit temperature increases with increasing the flow rate. For example the temperature increase from 67 ^oC to 73°C when the flow rate increases from 2.31 to 7.1 ml/s as shown in Figure 15a. This behaviour happens because, with higher velocity, a lower proportion of vapour is generated causing higher liquid fraction in the boiler, but with lower flow, more vapour generates which cannot be warmer than the saturation temperature and because the heat capacity of the liquid is higher than the vapour, then the liquid gains more thermal energy and becomes warmer. This is true for a certain limited range of flow rate, after that the average temperature of the solution should decrease with increasing velocity.

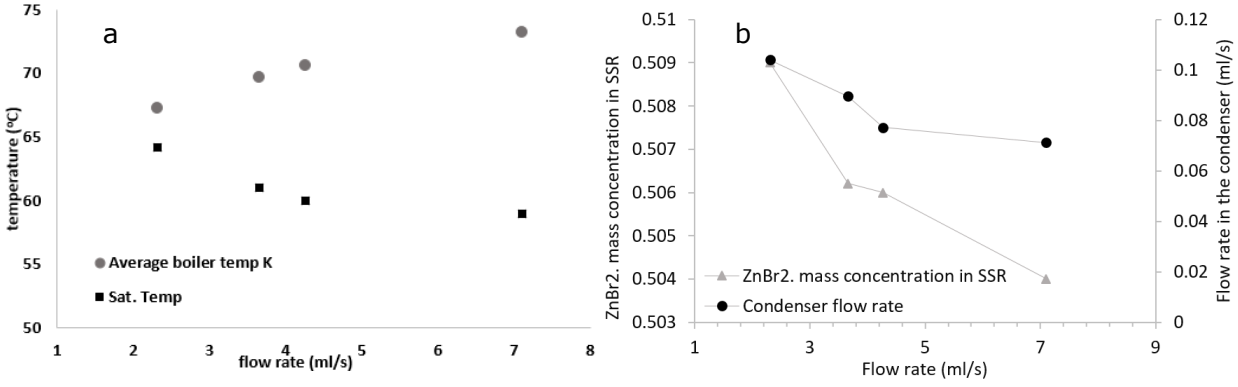

Figure 15: a- Relationship between the saturation temperature of acetone in the condenser and the average boiler temperature with the different flow rate. b- Relationship between the $ZnBr_2$ concentration in SSR and the condensed acetone flow rate in the condenser with the different flow rate. b-

Figure 15a also shows the temperature of the acetone vapour at entry to the condenser decreases with increasing flow rate. It decreased from 64 to 59 oC when the flow rate increased from 2.31 to 7.1 ml/s. This is because with increasing velocity, and consequent reduction in vapour generation there is a decrease in the pressure of the system and consequently of the saturation temperature. The concentration of the $ZnBr_2$ in the SSR becomes more than 50wt. % depending on the velocity with increasing flow rate. The concentration of the $ZnBr_2$ decreases due to evaporating more acetone which means with lower velocity, higher $ZnBr_2$ concentration in SSR as shown in Figure 15b. The condensed acetone flow rate decrease from 1.07 ml/s to 0.782 ml/s by increasing the flow rate in the boiler from 2.31 to 7.1 ml/s.

Conclusion

This study used a new nanofluid (nano-salt-fluid) acetone /$ZnBr_2$ based on graphene nanoparticles as the working fluid in the higher pressure part of a vapour absorption refrigeration system to look at how the different concentration of the nanoparticles (0 – 0.5 vol.%), boiler temperature (411, 418, 426, 436 and 446 K) and flow rate (2.31 - 7.1 ml/s) affect the behaviour of flow boiling. Also, the preparation and the properties of the new solution has been investigated. The results obtained can be summarized as:

Regarding the preparation and properties of the nanofluid, it was found that the stability of the acetone / $ZnBr_2$ based Graphene is mainly dependent on the density of the basefluid ($ZnBr_2$ concentration); the fluid is stable for 30 hours at 60 wt. %, and 8 hours at 50 wt. %. The density, thermal conductivity and viscosity increase with increasing the nanoparticles concentration, however the heat capacity decreases. The thermal conductivity increases by 4.5% with adding 0.5 vol. % of Graphene to the solution.

The Rohsenow constant of acetone / $ZnBr_2$ based Graphene on the stainless steel found as 0.217 depending on the Rohsenow nucleate boiling correlation and the power input. The stabilized pressure of the system will increase with increase in the concentration of the nanoparticles consequently, the saturation temperature increases also. An increasing relationship appears for increasing the heat flux and the heat transfer coefficient with increasing the particles loading. The condensing rate of acetone vapour is maximum at high concentration because of the high temperature difference of saturation and the wall temperature, consequently the concentration of the salt in the SSR increase. With increasing the boiler temperature the vapour generation increases which increases the pressure and the saturation temperature.

The heat flux and the heat transfer coefficient also rises with increasing $T_{wall} - T_{sat}$. The average solution temperature in the boiler increases with increasing the flow rate. Because with higher flow rate less vapour generates means more liquid exist in the boiler which means the fluid can gain more heat to become wormer. Higher flow rate makes the saturation temperature of the condenser decrease and consequently, the condensed acetone flow rate in the condenser drops then more salt concentration in the SSR existing. The general indication is that a small

proportion of nanoparticles can offer a benefit on providing improved boiling at lower temperatures where the temperature potential above saturation reduces.

Acknowledgement

This work was funded by The Higher Committee for Education Development (HCED), Iraq, by sponsorship reference D-12-1257 through the PhD Fellowship of the first author. Also, I would like to express my very great appreciation to University of Garmian for their support.

References

1. Suganthi, K., V.L. Vinodhan, and K. Rajan, *Heat transfer performance and transport properties of ZnO–ethylene glycol and ZnO–ethylene glycol–water nanofluid coolants.* Applied Energy, 2014. **135**: p. 548-559.
2. Barber, J., D. Brutin, and L. Tadrist, *A review on boiling heat transfer enhancement with nanofluids.* Nanoscale research letters, 2011. **6**(1): p. 1.
3. Saver, E.G.E. *Air Conditioning*. 5Mar. 2017; Available from: https://energy.gov/energysaver/air-conditioning.
4. Fang, X., et al., *A review of flow boiling heat transfer of nanofluids.* Applied Thermal Engineering, 2015. **91**: p. 1003-1017.
5. Bejan, A. and A.D. Kraus, *Heat transfer handbook*. Vol. 1. 2003: John Wiley & Sons.
6. Das, S.K., N. Putra, and W. Roetzel, *Pool boiling of nano-fluids on horizontal narrow tubes.* International Journal of Multiphase Flow, 2003. **29**(8): p. 1237-1247.
7. Trisaksri, V. and S. Wongwises, *Nucleate pool boiling heat transfer of TiO2–R141b nanofluids.* International Journal of Heat and Mass Transfer, 2009. **52**(5): p. 1582-1588.
8. Milanova, D. and R. Kumar, *Role of ions in pool boiling heat transfer of pure and silica nanofluids.* Applied Physics Letters, 2005. **87**(23): p. 233107.
9. Bang, I.C. and S.H. Chang, *Boiling heat transfer performance and phenomena of Al 2 O 3–water nano-fluids from a plain surface in a pool.* International Journal of Heat and Mass Transfer, 2005. **48**(12): p. 2407-2419.
10. Soltani, S., S.G. Etemad, and J. Thibault, *Pool boiling heat transfer of non-Newtonian nanofluids.* International Communications in Heat and Mass Transfer, 2010. **37**(1): p. 29-33.
11. Kim, H., H.S. Ahn, and M.H. Kim, *On the Mechanism of Pool Boiling Critical Heat Flux Enhancement in Nanofluids.* Journal of Heat Transfer, 2010. **132**(6): p. 061501-061501-11.
12. Golubovic, M.N., et al., *Nanofluids and critical heat flux, experimental and analytical study.* Applied Thermal Engineering, 2009. **29**(7): p. 1281-1288.
13. Wen, D. and Y. Ding, *Experimental investigation into the pool boiling heat transfer of aqueous based γ-alumina nanofluids.* Journal of Nanoparticle Research, 2005. **7**(2-3): p. 265-274.
14. Kim, H., J. Kim, and M.H. Kim, *Effect of nanoparticles on CHF enhancement in pool boiling of nano-fluids.* International Journal of Heat and Mass Transfer, 2006. **49**(25): p. 5070-5074.
15. Milanova, D. and R. Kumar, *Heat Transfer Behavior of Silica Nanoparticles in Pool Boiling Experiment.* Journal of Heat Transfer, 2008. **130**(4): p. 042401-042401-6.
16. Coursey, J.S. and J. Kim, *Nanofluid boiling: The effect of surface wettability.* International Journal of Heat and Fluid Flow, 2008. **29**(6): p. 1577-1585.
17. Chopkar, M., et al., *Pool boiling heat transfer characteristics of ZrO2–water nanofluids from a flat surface in a pool.* Heat and Mass Transfer, 2008. **44**(8): p. 999-1004.

18. Vassallo, P., R. Kumar, and S. D'Amico, *Pool boiling heat transfer experiments in silica–water nano-fluids.* International Journal of Heat and Mass Transfer, 2004. **47**(2): p. 407-411.
19. Henderson, K., et al., *Flow-boiling heat transfer of R-134a-based nanofluids in a horizontal tube.* International Journal of Heat and Mass Transfer, 2010. **53**(5–6): p. 944-951.
20. Boudouh, M., H.L. Gualous, and M. De Labachelerie, *Local convective boiling heat transfer and pressure drop of nanofluid in narrow rectangular channels.* Applied Thermal Engineering, 2010. **30**(17): p. 2619-2631.
21. Lee, J. and I. Mudawar, *Assessment of the effectiveness of nanofluids for single-phase and two-phase heat transfer in micro-channels.* International Journal of Heat and Mass Transfer, 2007. **50**(3): p. 452-463.
22. Ahn, H.S., et al., *Experimental study of critical heat flux enhancement during forced convective flow boiling of nanofluid on a short heated surface.* International Journal of Multiphase Flow, 2010. **36**(5): p. 375-384.
23. Peng, H., et al., *Measurement and correlation of frictional pressure drop of refrigerant-based nanofluid flow boiling inside a horizontal smooth tube.* International Journal of Refrigeration, 2009. **32**(7): p. 1756-1764.
24. Peng, H., et al., *Heat transfer characteristics of refrigerant-based nanofluid flow boiling inside a horizontal smooth tube.* International Journal of Refrigeration, 2009. **32**(6): p. 1259-1270.
25. Kim, S.J., et al., *Subcooled flow boiling heat transfer of dilute alumina, zinc oxide, and diamond nanofluids at atmospheric pressure.* Nuclear Engineering and Design, 2010. **240**(5): p. 1186-1194.
26. Kim, T.I., Y.H. Jeong, and S.H. Chang, *An experimental study on CHF enhancement in flow boiling using Al2O3 nano-fluid.* International Journal of Heat and Mass Transfer, 2010. **53**(5): p. 1015-1022.
27. Fang, X., et al., *Heat transfer and critical heat flux of nanofluid boiling: A comprehensive review.* Renewable and Sustainable Energy Reviews, 2016. **62**: p. 924-940.
28. Xu, L. and J. Xu, *Nanofluid stabilizes and enhances convective boiling heat transfer in a single microchannel.* International Journal of Heat and Mass Transfer, 2012. **55**(21): p. 5673-5686.
29. Kedzierski, M.A. and M. Gong, *Effect of CuO nanolubricant on R134a pool boiling heat transfer.* International Journal of Refrigeration, 2009. **32**(5): p. 791-799.
30. Kedzierski, M.A., *Effect of Al2O3 nanolubricant on R134a pool boiling heat transfer.* International Journal of Refrigeration, 2011. **34**(2): p. 498-508.
31. Peng, H., et al., *Effect of nanoparticle size on nucleate pool boiling heat transfer of refrigerant/oil mixture with nanoparticles.* International Journal of Heat and Mass Transfer, 2011. **54**(9): p. 1839-1850.
32. Sun, B. and D. Yang, *Flow boiling heat transfer characteristics of nano-refrigerants in a horizontal tube.* International Journal of Refrigeration, 2014. **38**: p. 206-214.
33. Kim, S.J., et al., *Alumina Nanoparticles Enhance the Flow Boiling Critical Heat Flux of Water at Low Pressure.* Journal of Heat Transfer, 2008. **130**(4): p. 044501-044501.
34. *Role of ions in pool boiling heat transfer of pure and silica nanofluids.* Applied Physics Letters, 2005. **87**(23): p. 233107.
35. Bang, I.C. and S. Heung Chang, *Boiling heat transfer performance and phenomena of Al2O3–water nano-fluids from a plain surface in a pool.* International Journal of Heat and Mass Transfer, 2005. **48**(12): p. 2407-2419.
36. Das, S.K., N. Putra, and W. Roetzel, *Pool boiling characteristics of nano-fluids.* International journal of heat and mass transfer, 2003. **46**(5): p. 851-862.
37. Zhou, D.W., *Heat transfer enhancement of copper nanofluid with acoustic cavitation.* International Journal of Heat and Mass Transfer, 2004. **47**(14): p. 3109-3117.

38. *Effect of nanoparticles on critical heat flux of water in pool boiling heat transfer.* Applied Physics Letters, 2003. **83**(16): p. 3374-3376.
39. Abedini, E., et al., *Experimental investigation and comparison of subcooled flow boiling of TiO2 nanofluid in a vertical and horizontal tube.* Proceedings of the Institution of Mechanical Engineers, Part C: Journal of Mechanical Engineering Science, 2013. **227**(8): p. 1742-1753.
40. Witharana, S., *Boiling of refrigerants on enhanced surfaces and boiling of nanofluids.* Sweden: Royal Institute of Technology, Stockholm, 2003.
41. Sun, B. and D. Yang, *Flow boiling heat transfer characteristics of nano-refrigerants in a horizontal tube.* International Journal of Refrigeration, 2014. **38**(Supplement C): p. 206-214.
42. Rana, K.B., A.K. Rajvanshi, and G.D. Agrawal, *A visualization study of flow boiling heat transfer with nanofluids.* Journal of Visualization, 2013. **16**(2): p. 133-143.
43. Rana, K.B., et al., *Measurement of void fraction in flow boiling of ZnO–water nanofluids using image processing technique.* Nuclear Engineering and Design, 2014. **270**(Supplement C): p. 217-226.
44. Nikkhah, V., M.M. Sarafraz, and F. Hormozi, *Application of Spherical Copper Oxide (II) Water Nano-fluid as a Potential Coolant in a Boiling Annular Heat Exchanger.* Chemical and biochemical engineering quarterly, , 2015. **29(3)**: p. 11.
45. Joel A W Hamilton, *Investigation into discontinuous low temperature waste heat utilisation from a renewable power plant in rural India for absorption refrigeration*. 2016, The University of Nottingham.
46. Mohammed, H.I., D. Giddings, and G.S. Walker, *CFD simulation of a concentrated salt nanofluid flow boiling in a rectangular tube.* International Journal of Heat and Mass Transfer, 2018. **125**: p. 218-228.
47. Ajib, S. and A. Karno, *Thermo physical properties of acetone–zinc bromide for using in a low temperature driven absorption refrigeration machine.* Heat and Mass Transfer, 2008. **45**(1): p. 61-70.
48. Peyghambarzadeh, S., et al., *Experimental study of heat transfer enhancement using water/ethylene glycol based nanofluids as a new coolant for car radiators.* International Communications in Heat and Mass Transfer, 2011. **38**(9): p. 1283-1290.
49. Zhou, S. and R. Ni, *Measurement of the specific heat capacity of water-based Al~ 2O~ 3 nanofluid.* Applied Physics Letters, 2008. **92**(9): p. 093123.
50. Bejan, A., *CONVECTION HEAT TRANSFER*. 2003, John Wiley & Sons. p. 378.
51. Jabardo, J.M.S., et al., *Evaluation of the rohsenow correlation through experimental pool boiling of halocarbon refrigerants on cylindrical surfaces.* Journal of the Brazilian Society of Mechanical Sciences and Engineering, 2004. **26**: p. 218-230.
52. Choon, N.K., et al., *New pool boiling data for water with copper-foam metal at sub-atmospheric pressures: Experiments and correlation.* Applied Thermal Engineering, 2006. **26**(11): p. 1286-1290.
53. , T.E.T. *Fluids - Latent Heat of Evaporation*. 5/2/2018]; Available from: https://www.engineeringtoolbox.com/fluids-evaporation-latent-heat-d_147.html.
54. Stievano, M. and N. Elvassore, *High-pressure density and vapor–liquid equilibrium for the binary systems carbon dioxide–ethanol, carbon dioxide–acetone and carbon dioxide–dichloromethane.* The Journal of Supercritical Fluids, 2005. **33**(1): p. 7-14.
55. Jasper, J.J., *The Surface Tension of Pure Liquid Compounds.* Journal of Physical and Chemical Reference Data, 1972. **1**(4): p. 841-1010.
56. Soni, M., D. Ramjugernath, and J.D. Raal, *Vapor–Liquid Equilibrium for Binary Systems of 2,3-Pentanedione with Diacetyl and Acetone.* Journal of Chemical & Engineering Data, 2008. **53**(3): p. 745-749.
57. PASS. *GE Druck UNIK 5000 Configurable Silicon Pressure Sensor*. 2018 [cited 2018 2nd / Feb.]; Available from: https://www.tester.co.uk/ge-druck-unik-5000-configurable-silicon-pressure-sensor?gclid=Cj0KCQiAgs7RBRDoARIsANOo-

Hju4tUEFtWix4ATBBFidR5Y-x7LBxtuOiOQZWXPfgqxWI9DuS98TdcaAhzkEALw_wcB.
58. Eastman, J.A., et al., *THERMAL TRANSPORT IN NANOFLUIDS.* Annual Review of Materials Research, 2004. **34**(1): p. 219-246.
59. Evans, W., J. Fish, and P. Keblinski, *Role of Brownian motion hydrodynamics on nanofluid thermal conductivity.* Applied Physics Letters, 2006. **88**(9): p. 093116.
60. Koo, J. and C. Kleinstreuer, *Impact analysis of nanoparticle motion mechanisms on the thermal conductivity of nanofluids.* International Communications in Heat and Mass Transfer, 2005. **32**(9): p. 1111-1118.
61. Wang, X., X. Xu, and S.U. S. Choi, *Thermal Conductivity of Nanoparticle - Fluid Mixture.* Journal of Thermophysics and Heat Transfer, 1999. **13**(4): p. 474-480.
62. You, S., J. Kim, and K. Kim, *Effect of nanoparticles on critical heat flux of water in pool boiling heat transfer.* Applied Physics Letters, 2003. **83**(16): p. 3374-3376.
63. Narayan, G.P., K.B. Anoop, and S.K. Das, *Mechanism of enhancement/deterioration of boiling heat transfer using stable nanoparticle suspensions over vertical tubes.* Journal of Applied Physics, 2007. **102**(7): p. 074317.
64. Bolukbasi, A., D. Ciloglu, and B. Sahin, *The Characteristic Pool Boiling Curves of Nanofluids.* World Academy of Science, Engineering and Technology, 2012. **67**: p. 163-165.
65. Zhou, D., *Heat transfer enhancement of copper nanofluid with acoustic cavitation.* International Journal of Heat and Mass Transfer, 2004. **47**(14): p. 3109-3117.
66. Suriyawong, A. and S. Wongwises, *Nucleate pool boiling heat transfer characteristics of TiO2–water nanofluids at very low concentrations.* Experimental Thermal and Fluid Science, 2010. **34**(8): p. 992-999.
67. Lee, S.W., K.M. Kim, and I.C. Bang, *Study on flow boiling critical heat flux enhancement of graphene oxide/water nanofluid.* International Journal of Heat and Mass Transfer, 2013. **65**(Supplement C): p. 348-356.